Propagation of nonlinear pulses in chirped fiber gratings

E. N. Tsoy* and C. M. de Sterke
School of Physics, The University of Sydney, New South Wales 2006, Australia
(Received 7 December 1999)

The propagation of nonlinear optical pulses in chirped fiber gratings is studied. The dynamics is analyzed on the basis of the inhomogeneous nonlinear Schrödinger equation. By using perturbation theory we demonstrate that the inhomogeneity affects the amplitude and the width, as well as the phase and the velocity of the soliton. The dynamics of a multisoliton pulse (breather) in chirped gratings is also discussed. It is shown that the velocity variation of individual solitons leads to the breaking of a bound multisoliton state. This process manifests itself as the pulse splitting that is experimentally observed by other authors. Numerical simulations of the pulse dynamics agree well with analytical results for wide range of parameters.

PACS number(s): 42.79.Dj, 42.81.Dp

I. INTRODUCTION

There is an increasing theoretical and experimental interest in pulse propagation in Bragg gratings [1]. The large group velocity dispersion, the selective frequency response, and the nonlinear properties of gratings allow applications such as in-fiber filters, dispersion compensation devices [2], pulse compressors [3], and sensors [4].

In fiber Bragg gratings, in which the refractive index in the fiber core varies (almost) periodically as a function of position, the forward and backward propagating waves are strongly coupled. This leads to the opening of a photonic band gap in the optical spectrum, and low group velocity and strong dispersion for frequencies just outside this gap. The high-intensity dynamics of the forward and backward propagating waves is described by the nonlinear coupled mode equations (NLCMEs). However, a convenient and adequate description can also be given using the nonlinear Schrödinger (NLS) equation [5]. Both these equations have soliton solutions that can propagate at velocities well below the speed of light in the uniform medium. Indeed, the existence of such ''grating solitons'' was verified experimentally by Eggleton *et al.* [5,6], Taverner *et al.* [7], and Millar *et al.* [8].

Nonuniform gratings, which are characterized by variations of the local Bragg frequency (chirped gratings) or variations in the grating strength, have additional degrees of freedom for the control of pulse propagation. The present work is motivated by the experiments of Slusher *et al.* [9], who studied high-intensity propagation in linearly chirped gratings. They found that incident pulses with a peak intensity exceeding roughly 10 GW/cm^2 that are reflected by such a grating split into a pair of pulses under very general conditions. An example of such a dynamics is given in Fig. 1.

We analyze pulse propagation in nonuniform gratings, including the pulse splitting, using the reduction of the NLCMEs to the NLS equation (Sec. II A) [10,11]. Applying perturbation theory we first study the dynamics of single solitons, and show that the inhomogeneity affects the soliton amplitude and width, as well as its velocity and frequency (Sec. II B). As a consequence of this, we find that higher-order solitons propagating in nonuniform gratings split (Sec. II C). In Sec. III this insight is used to explain the results of Slusher *et al.* [9]: an incident pulse that is sufficiently intense splits into its soliton components. For most two-soliton pulses, the peak intensities of the emerging solitons differ by an order of magnitude, so that, in effect, a single pulse is observed experimentally. Only three-soliton pulses, and two soliton pulses close to the three-soliton threshold, lead to soliton components with roughly similar intensity ratios, which can thus be observed separately. This is confirmed by numerical simulations, which show that the threshold for splitting approximately corresponds to that for three-soliton formation. The dynamics of a two-soliton pulse of the perturbed NLS equation is analyzed numerically in the Appendix by using the inverse scattering transform (IST) method.

II. THEORY

The refractive index of a nonuniform grating is written as

$$n(z)=\bar{n}+\delta n(z)+\Delta n(z)\cos\left(\frac{2\pi z}{d}+\theta(z)\right), \qquad (1)$$

where $\bar{n}$ is the average refractive index, δn is the variation in the background refractive index, Δn is the modulation depth of the grating, d is the nominal grating period, and θ is its phase. Assuming $\delta n, \Delta n$ small ($\ll \bar{n}$) and all slowly varying, the envelope functions $\mathcal{E}_{\pm}$ of the electric field are known to obey the NLCMEs [10]

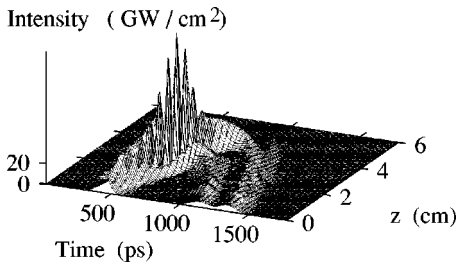

FIG. 1. The evolution of the total intensity inside the chirped grating, $L=0.06$ m, $\sigma=1700$ m^{-1}, $I_{inc}=20$ GW/cm^2.

*Also at the Physical-Technical Institute of the Uzbek Academy of Sciences, 2-B, Mavlyanova Str., Tashkent, 700084, Uzbekistan.

$$\frac{i}{V}\frac{\partial \mathcal{E}_{\pm}}{\partial t} \pm i\frac{\partial \mathcal{E}_{\pm}}{\partial z} + \delta(z)\mathcal{E}_{\pm} + \kappa(z)\mathcal{E}_{\mp} + \Gamma(|\mathcal{E}_{\pm}|^2 + 2|\mathcal{E}_{\mp}|^2)\mathcal{E}_{\pm} = 0, \tag{2}$$

where the subscript corresponds to forward $(+)$ and backward $(-)$ propagating waves, V is the group velocity in the grating's absence, $\Gamma = 4\pi\bar{n}n_2/(\lambda_B Z)$, n_2 is the nonlinear refractive index, $\lambda_B = 2\bar{n}d$ is the Bragg wavelength, and Z is the vacuum impedance. The grating strength $\kappa(z)$ and the variation of the local Bragg frequency $\delta(z)$ are given by

$$\kappa(z) = \frac{\pi}{\lambda_B}\Delta n(z), \quad \delta(z) = \frac{2\pi}{\lambda_B}\delta n(z) - \frac{1}{2}\frac{d\theta}{dz}. \tag{3}$$

The dispersion relation ($\mathcal{E}_{\pm} \sim \exp[i(Qz - \Omega t)]$) of uniform linear gratings has two branches, and is given by

$$\Omega_{\pm} = V(-\delta \pm \sqrt{\kappa^2 + Q^2}). \tag{4}$$

The dimensionless group velocity v is

$$v \equiv \frac{1}{V}\frac{d\Omega_{\pm}}{dQ} = \pm\frac{Q}{\sqrt{Q^2+\kappa^2}}. \tag{5}$$

In nonuniform gratings that are sufficiently slowly varying, Q, and v can be considered as local parameters.

A. Nonlinear Schrödinger equation

Though the NLCMEs (2) govern wave propagation in gratings, perturbation theory is not well developed for these equations. We therefore use the reduction of the NLCMEs to the NLS equation, which is very well studied. Consider the eigenfunctions (Bloch functions) corresponding to the dispersion relation (4),

$$f_u = \frac{1}{\sqrt{2}}\begin{pmatrix} \sqrt{1+v} \\ -\sqrt{1-v} \end{pmatrix}, \quad f_l = \frac{1}{\sqrt{2}}\begin{pmatrix} \sqrt{1-v} \\ \sqrt{1+v} \end{pmatrix}, \tag{6}$$

where f_u (f_l) refers to the upper (lower) branch of the dispersion relation. Note that Eqs. (4) and (5) only specify $|v|$, and not its sign. Therefore, for forward propagating (incoming) pulses we take $v>0$, whereas for backward propagating (reflected) pulses we take $v<0$. We now write a multiscale expansion of the envelopes as [1]

$$\begin{pmatrix} \mathcal{E}_+ \\ \mathcal{E}_- \end{pmatrix} = \Big[\nu a(z_j,t_j) f_u(z_j) + \nu^2 b_1(z_j,t_j) f_l(z_j) + \nu^3 b_2(z_j,t_j) f_l(z_j) \exp\Big[i\Big(\int_0^z Q(z)dz - \Omega_+ t \Big)\Big], \tag{7}$$

where $z_j = \nu^j z$, $t_j = \nu^j t$, $j = 1,2,\ldots$, and $\nu \ll 1$ is a small parameter. Slow variations of the Bloch functions via the z_j have to be included in this expression to account for the grating nonuniformity [10,11]. Substituting Eq. (7) into Eq. (2) and applying multiple scale analysis, one obtains in order ν^3 the perturbed NLS equation for the complex amplitude of the Bloch function $a(z,t)$ [10,11]

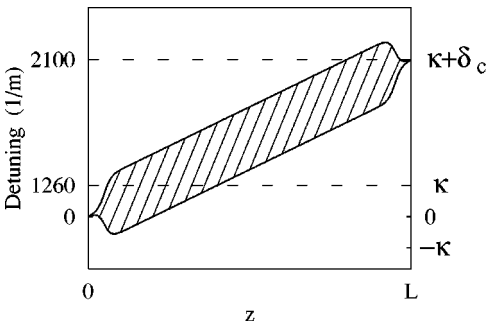

FIG. 2. The band diagram of apodized chirped ($\alpha<0$) gratings as a function of the detuning $\sigma=(\omega-\omega_B)/V$ and the distance z. Numbers near the left axis correspond to the set of parameters, used in numerical simulations. In the work of Slusher *et al.* [9] $\kappa = 1260\ \mathrm{m}^{-1}$, $L = 6$ cm.

$$iv\frac{\partial a}{\partial z} + \frac{i}{V}\frac{\partial a}{\partial t} + \frac{1}{2\kappa\gamma^3 v^2 V^2}\frac{\partial^2 a}{\partial t^2} + \frac{\Gamma(3-v^2)}{2}|a|^2 a = -\frac{i}{2}v'a - \frac{1}{2\kappa\gamma v V}\left(\frac{\kappa'}{\kappa\gamma^2} + \frac{(2+v^2)v'}{v}\right)\frac{\partial a}{\partial t} - \frac{1}{4\kappa v}\left(\frac{v'\kappa'}{\kappa\gamma} + \frac{\gamma(3-2v^2)v'^2}{2v} - \frac{v''}{\gamma}\right)a, \tag{8}$$

where $v(z)V$ is the local group velocity, $\gamma = 1/\sqrt{1-v^2}$, and the prime means the space derivative d/dz. Equation (8) describes pulse propagation for frequencies *outside* the band gap at any grating position; for incoming pulses $v>0$, for reflected pulses $v<0$. The equation is valid for any type of nonuniformity. The propagation of pulses in chirped gratings ($\kappa=$const) or in gratings with variable strength ($\delta=$const) can be obtained as particular cases. The relations between v, δ, and κ and their variations are [10]

$$v = \sqrt{1 - \frac{\kappa^2}{(\Omega_+/V + \delta)^2}}, \qquad \frac{dv}{dz} = \frac{1}{\kappa\gamma^3 v}\frac{d\delta}{dz} - \frac{1}{\kappa\gamma^2 v}\frac{d\kappa}{dz}. \tag{9}$$

Though our formalism is completely general, let us consider here the type of gratings of direct interest. Shown in Fig. 2 is the band diagram of an apodized, chirped grating with the total chirp δ_c. The frequencies at which the field envelopes are evanescent, and where the grating thus reflects, are indicated by the dashed lines. The apodized regions at the front and the back reduce out-of-band reflections. The grating's central section is chirped but has a uniform strength; this section is the main focus of this work.

Now we find the relation between the incident pulse and the initial condition at the start of the central section $a(0,t)$. These differ because of the taper [5]. We assume the spectrum of the incident pulse to be outside the band gap, so that essentially all incoming energy transforms to the forward propagating pulse in the grating and reflections are negligible. Let the envelope of the incident pulse at $z=0$ have the form

$$\mathcal{E}_{inc}(t)=\mathcal{E}_0\,\mathrm{sech}(t/\tau_0)\exp(-i\sigma Vt), \tag{10}$$

where τ_0 is the pulse duration, ω is the carrier frequency, ω_B is the Bragg frequency at $z=0$, and $\sigma=(\omega-\omega_B)/V=\Omega_+/V$ is the detuning. We suppose that in the tapers the pulse transforms *adiabatically*, affecting only its amplitude. Then from the linearized Eq. (8), and using leading terms, we find [11]

$$a(z\approx 0,t)=\frac{\mathcal{E}_0}{\sqrt{v(0)}}\,\mathrm{sech}(t/\tau_0). \tag{11}$$

The same relation can be obtained from the conservation law $dJ/dz=0$, where $J\equiv\int_{-\infty}^{\infty}(|\mathcal{E}_+|^2-|\mathcal{E}_-|^2)\,dt$. Thus, the total field intensity inside the grating is larger than that outside by a factor $1/v(0)$. Though numerical simulations show that there is also a variation of the pulse phase during propagation through the taper, relation (11) is a good approximation for a large set of system parameters.

We now analyze the pulse dynamics using Eq. (8). First note that the peak intensity of the incident pulse (10), corresponding to the fundamental soliton in a *uniform* grating is [5]

$$I_f=\frac{3.107}{V^2}\,\frac{\lambda_B}{\pi\kappa n_2 w^2 v\,\gamma^3(3-v^2)}, \tag{12}$$

where w is the full width at half maximum (FWHM), related to τ_0 from Eq. (11) as $w=2\tau_0\cosh^{-1}(\sqrt{2})$. The threshold I_N for the creation of N solitons from the pulse with initial shape (10) is related to I_f by [12] $I_N=(N-1/2)^2 I_f$. The intensity I_f depends on the detuning through v, so we use it for estimates of thresholds for nonuniform gratings as well.

Below we drop the last term on the right-hand side of Eq. (8) because the coefficient in brackets is small for typical values of the parameters. Moreover, the last term can be eliminated by a phase transformation of the field $a(z,t)$.

Since the grating nonuniformity leads to the position dependence of the dispersion and nonlinearity, it is convenient to introduce new dimensionless variables

$$y=\int_0^z\frac{dz}{z_s},\quad \tau=\frac{1}{\tau_0}\left(t-\frac{1}{V}\int_0^z\frac{dz}{v}\right),\quad \psi=\frac{a}{a_s}, \tag{13}$$

where

$$z_s(z)=\tau_0^2V^2\kappa\gamma^3v^3,\qquad a_s(z)=\sqrt{2}/[vV\tau_0\sqrt{\gamma^3\kappa\Gamma(3-v^2)}]. \tag{14}$$

Here z_s is the scale of the propagation distance, which equals the dispersion length, and a_s is the amplitude scale of the field ψ [$a_s(0)$ is the amplitude of the *fundamental* soliton, cf. Eq. (12)]. With increasing v, a_s decreases, while z_s increases. Then Eq. (8) can be written in its final form

$$i\psi_y+\frac{1}{2}\psi_{\tau\tau}+|\psi|^2\psi=-i\epsilon_0\psi-\epsilon_1\psi_\tau, \tag{15}$$

where

$$\epsilon_0=\frac{v_y}{2v}+\frac{a_{s,y}}{a_s},\qquad \epsilon_1=\frac{1}{2\gamma v^2V\kappa\tau_0}\left(\frac{\kappa_y}{\kappa\gamma^2}+\frac{(2+v^2)v_y}{v}\right). \tag{16}$$

We should mention that equations similar to Eq. (15) have been studied in the context of soliton propagation in optical fibers [13], e.g., in fibers with losses and in dispersion-decreasing fibers.

B. Dynamics of a single soliton

Here we consider the effect of the perturbation terms ϵ_0 and ϵ_1, due to the grating's inhomogeneity, on the dynamics of the single soliton

$$\psi(y,\tau)=A(y)\,\mathrm{sech}(x)\exp(i\varphi), \tag{17}$$

where

$$x=[\tau-\tau_c]/\tau_p,\quad \varphi=\phi+c_1\tau_p x+c_2\tau_p^2x^2.$$

Here τ_c, τ_p, ϕ, c_1, and c_2 are functions of y. The values $-\Omega_++c_1/\tau_0$ and c_2/τ_0^2 are the linear phase and the chirp coefficients of the pulse envelope, respectively. Below we deal only with slow inhomogeneities, so that the perturbations in Eq. (15) are small. Therefore, we assume that the inhomogeneity only results in a variation of soliton parameters without changing the shape. To obtain the equations for the parameter evolution we use the perturbation method of Maimistov [14], according to which

$$\frac{d}{dy}(\tau_pA^2)=-2\left(\epsilon_1c_1+\frac{v_y}{2v}+\frac{a_{s,y}}{a_s}\right)\tau_pA^2, \tag{18}$$

$$\frac{d\tau_c}{dy}=c_1-\frac{\pi^2}{3}\epsilon_1c_2\tau_p^2, \tag{19}$$

$$\frac{dc_1}{dy}=-\frac{2\epsilon_1}{3\tau_p^2}(1+\pi^2c_2^2\tau_p^4), \tag{20}$$

$$\frac{dc_2}{dy}=2\left(\frac{1}{\pi^2\tau_p^4}-c_2^2-\frac{A^2}{\pi^2\tau_p^2}\right), \tag{21}$$

$$\frac{d\tau_p}{dy}=2c_2\tau_p. \tag{22}$$

According to Eqs. (18)–(22), the inhomogeneity affects the soliton center τ_c and the frequency shift c_1. We use this in discussing the splitting of a bound state of soliton (see Sec. II C). By the definition of $\psi(y,\tau)$, the initial linear phase coefficient $c_1(0)=0$ [see Eqs. (11) and (13)]. Hence for small distances $y\ll 1/\epsilon_1$, the coefficient $c_1(y)\sim O(\epsilon_1)$, and the first term on the right-hand side of Eq. (18) can be dropped as $O(\epsilon_1^2)$. Then Eq. (18) can be immediately integrated, giving

$$\frac{\tau_p A^2}{\tau_{p0} A_0^2} = \frac{a_{s0}^2 v_0}{a_s^2 v}, \tag{23}$$

where subscript ''0'' denotes the initial value of corresponding parameter, i.e., at $y=0$. The product $\tau_p A^2$ is a measure of the total pulse power. Therefore Eq. (23) represents variations of the pulse power due to the inhomogeneity. In dimensional units Eq. (23) has the form

$$t_p a_m^2 = \frac{\tau_0 \mathcal{E}_0^2}{v}, \tag{24}$$

where t_p is the local pulse width, and a_m is the maximum of the absolute value of the Bloch function envelope $|a(z,t)|$ [see Eq. (7)]. Note that an inhomogeneity with $v_z<0$ ($v_z>0$) in the actual system has the same effect as a variable dissipation (amplification) in the dimensionless system. Since both z_s and a_s [Eq. (14)] also change due to the inhomogeneity, variations of the actual envelope $a(z,t)$ cannot be easily predicted. There is of course no energy loss or gain due to the inhomogeneity, and the quantity J (see Sec. II A) does not vary with position.

Combining Eqs. (21) and (22) and taking into account Eq. (23), we obtain the equation for the pulse duration

$$\frac{d^2\tau_p}{dy^2} = \frac{4}{\pi^2}\left[\frac{1}{\tau_p^3} - A_0^2 \frac{a_{s0}^2 v_0}{a_s^2 v}\frac{1}{\tau_p^2}\right], \tag{25}$$

with the following initial conditions:

$$\tau_p(0)=1, \quad d\tau_p(0)/dy = 2c_2(0). \tag{26}$$

The remaining parameters of the soliton are determined from $\tau_p(y)$. Equation (25) is a Kepler equation with varying coefficient. A similar equation was studied by Anderson [15] in the context of optical soliton propagation in media with *constant* dissipation, while in our case the perturbation coefficients vary on y. We give here only the main conclusions from the analysis of Eq. (25), which is similar to that of Anderson [15]. First of all, depending on the sign of the Hamiltonian H of Eq. (25), which is defined as

$$H = \frac{1}{2}\left(\frac{d\tau_p}{dy}\right)^2 + \left[\frac{2}{\pi^2\tau_p^2} - 4A_0^2 \frac{a_{s0}^2}{a_s^2}\frac{v_0}{v}\frac{1}{\pi^2\tau_p}\right], \tag{27}$$

the pulse width either oscillates ($H<0$) about $\tau_{min} = a_s^2 v/[A_0^2 a_{s0}^2 v_0]$, the minimum of the effective Kepler potential, or asymptotically grows ($H>0$). One finds that both H and $\tau_{\min}$ increase when v decreases and vice versa. It means that due to inhomogeneity the regime of the width dynamics changes with the propagation. The period of the width oscillations, corresponding to the period of motion on the elliptic orbit of Kepler potential [16], depends on the position inside the grating as

$$Z_p(y) = \frac{4}{\pi}\frac{a_{s0}^2 v_0}{a_s^2 v^2}\frac{A_0^2}{\sqrt{2|H|^3}}. \tag{28}$$

For $c_2(0)=0$, the initial period of *small* oscillations Z_s is calculated as $Z_p(0)$ with the additional condition $A_0=1$ (the initial pulse is close to the fundamental soliton), so that $Z_s=\pi^2$ in units of the dispersion length. We note that the treatment given here does not include radiation losses, which cause the oscillations around $\tau_{\min}$ to be damped. As an aside, we also mention that if the inhomogeneity is periodic with the period close to Z_p, then resonance and chaotic phenomena can occur, leading to pulse broadening and even pulse breaking [17].

The previous arguments are sufficient for a qualitative description of the pulse behavior during the propagation inside the inhomogeneous grating. Moreover, the solution of Eq. (25) can easily be found numerically. However, here we consider limiting cases to obtain some explicit relations. Though the relations above are valid both for $\delta=\delta(z)$ and $\kappa=\kappa(z)$, below we concentrate on chirped gratings, keeping $\kappa=$const. We introduce, in addition to Z_p, two characteristic dimensionless lengths—the length of the system Z_L and the chirp length Z_c

$$Z_L(L) = \frac{1}{\kappa V^2 \tau_0^2}\int_0^L (\gamma v)^{-3} dz,$$
$$Z_c(y) = \left|\frac{v(3-v^2)}{3\gamma^2(1+v^2)}\frac{dy}{dv}\right|. \tag{29}$$

The length scale Z_c is defined as the scale of the varying coefficient, which is the inverse local asymptotic width $1/\tau_{min}$ in Eq. (25).

The first limiting case is that of short gratings $Z_L \ll Z_p$, where the variations of the pulse width is small. Then Eq. (25) can be approximated as

$$\frac{d^2\tau_p}{dy^2} = \frac{4}{\pi^2}\left[1 - A_0^2\frac{a_{s0}^2 v_0}{a_s^2 v}\right], \tag{30}$$

so that the pulse width is completely determined by the inhomogeneity. For short gratings, if the amplitude of the incident pulse is greater (less) than the amplitude of the fundamental soliton, $A_0>1$ ($A_0<1$), then τ_p decreases (increases) for any weak inhomogeneity.

The next limiting case is that of adiabatic dynamics, $Z_c \gg Z_p$, when the Kepler potential changes slowly compared with the oscillation period. By applying the WKB method (see also the work by Anderson [15]) we find

$$\tau_p = \tau_{min}\left[1 + \beta\cos\left(\frac{2}{\pi}\int_0^y \tau_{min}^{-2} dy + \vartheta_0\right)\right], \tag{31}$$

where constants β and ϑ_0 are determined from the set

$$A_0^2 - 1 = \beta\cos\vartheta_0,$$
$$2c_{20} - A_0^2\frac{d\tau_{min}(0)}{dy} = -\frac{2}{\pi}A_0^2\beta\sin\vartheta_0. \tag{32}$$

The second term in Eq. (31) is negligible, if the incident pulse is close to a fundamental soliton, i.e., $A_0=1$.

Let us now apply these results to *linearly* chirped gratings $\delta=\alpha z$, where α is a constant. The characteristic lengths then have the following forms:

$$Z_c=\frac{1}{V^2\tau_0^2\alpha}\,\frac{3-v^2}{3v\,\gamma^2(1+v^2)},$$
$$Z_L=\frac{1}{V^2\tau_0^2\alpha}\left(\frac{1}{v_0}-\frac{1}{v(L)}\right). \tag{33}$$

The adiabatic dynamics is described by [see Eq. (31)]

$$\tau_p=\tau_{min}\{1+\beta\cos[\mu(f(v)-f(v_0))+\vartheta_0]\}, \tag{34}$$

where

$$\mu=\frac{[a_{s0}^2A_0^2v_0V\tau_0\kappa\Gamma]^2}{8\pi\alpha},$$

$$f(v)=\frac{2v(9-7v^2)}{(1-v^2)^2}+9\ln\frac{1+v}{1-v}.$$

Therefore the soliton width, as well as other soliton parameters, oscillates about the value corresponding to the asymptotic soliton. This value and the frequency of oscillations changes slowly with the position.

Let us discuss the validity of Eqs. (18)–(22) and (25). As any perturbation theory the approach is correct when the variation of the parameters and/or their derivatives is small enough. Therefore the results apply to slow inhomogeneities and sufficiently short gratings. Estimates show that for the chirp slope $\alpha\sim 10^3$ m^{-2}, the range of admitted velocities v is $0.3\lesssim v\lesssim 0.9$, which corresponds to detunings between $1.05\,\kappa$ and $2.3\,\kappa$. For smaller velocities the local wave number is also small, so that the assumption of a slowly varying envelope [see Eq. (7)] breaks down. For velocities v close to unity the dispersion length z_s becomes large, so that this analysis is also not valid. The reduction of the system (18)–(22) to the second-order ordinary differential equation (25) is allowed for short systems $Z_L\ll 1/\epsilon_1$. For larger systems one should solve the whole set (18)–(22), though the pulse behavior is qualitatively similar.

C. Dynamics of multisoliton pulses

We are particularly interested in the application to multisoliton pulses as observed in experiments of Slusher *et al.* [9]. It is known that for the unperturbed NLS equation the initial condition (17) with $\varphi=0$ and arbitrary amplitude A produces the bound state of N solitons (pure imaginary eigenvalues ζ_j) with corresponding amplitudes [12] $\psi_{0j}=2\eta_j=2(A-j)+1$, where $j=1,\ldots,N$ and N is the largest positive integer, satisfying $2(A-N)+1>0$. The threshold for the N soliton creation is $A_N=N-1/2$. Suppose that due to some perturbations the bound state splits into several, closely spaced pulses. Since the intensity is proportional to the square of the amplitude, the ratio of peak intensities of the smallest and the largest solitons is $\sim(2A-2N+1)^2/(2A-1)^2$. For example, for $A=2$, $N=2$, the peak intensity of the smaller soliton is only roughly 10% of that of the larger soliton. Therefore, two-soliton solutions are observed as a single pulse up to $A\gtrsim 2$, while the three-soliton solution is seen as a two-pulse state for almost all corresponding values of A. Though it is possible that some perturbations create new solitons, the amplitudes of these solitons vanish, so that they are difficult to observe.

We saw from the analysis of the single soliton dynamics in Sec. II B, that the inhomogeneity leads to variations of the pulse position. In other words, the velocities of solitons in the bound state are not equal, resulting in pulse splitting. The dynamics of an N breather under perturbations is different from the dynamics of N separate solitons due to the strong mutual interaction. However, as shown in the Appendix, the dynamics of individual solitons in the two-soliton bound state is qualitatively the same as the dynamics of the single soliton. The perturbations affect the larger soliton more strongly and after the splitting the solitons move in opposite directions with respect to their ''center of mass.'' The important point is that the small perturbations do not create new solitons, even though their effects are similar to that of gain ($\epsilon_0<0$).

Recall that we assumed that the effect of the taper can be captured by Eq. (11). Numerical calculations in fact show that just after the taper, the pulses are slightly chirped. This initial chirp can result in increased thresholds for multisoliton creation [18].

III. COMPARISON WITH NUMERICAL SIMULATIONS AND EXPERIMENTS

To verify the theory, we consider the linearly chirped grating ($\delta=\alpha z,\alpha<0$) of length $L=6$ cm and with bandgap width 0.3 nm near the Bragg wavelength $\lambda_B=1053.2$ nm. The total grating chirp $\Delta\lambda_c$ is chosen equal to 0.02, 0.05, and 0.1 nm, where the total variation of the Bragg frequency δ_cV is related to $\Delta\lambda_c$ as $\delta_cV=|2\pi\bar{n}\Delta\lambda_c/\lambda_B^2|V$. The pulse width (FWHM) is 80 ps. These parameters are close to those of Slusher *et al.* [9]. Estimating the perturbations in Eq. (15), we find that in the cases considered, $|\epsilon_1|<|\epsilon_0|$ and

$$\epsilon_0=-\frac{3}{2}\alpha\tau_0^2V^2\gamma^2v\frac{1+v^2}{3-v^2}.$$

For a 6 cm grating, a total chirp $\Delta\lambda_c=0.1$ nm is not small, $\epsilon_0\sim O(1)$. However, as shown below, even for this case the theory is qualitatively correct.

Chirped gratings have a selective response depending on the detuning. Namely, for $\alpha<0$, waves with the initial detuning σ [see Eq. (10)], satisfying $\kappa<\sigma<\kappa+\delta_c$, are reflected, while waves with detuning $\sigma>\kappa+\delta_c$ propagate almost without reflection (see also Fig. 2). In fact, the dynamics of pulses is more complicated, especially for detunings close to $\kappa+\delta_c$, where part of the incident energy is reflected and the rest is transmitted.

First we consider the propagation of one-soliton pulses and present results for the transmission, when the initial detuning is outside the gap, $\sigma>\kappa+\delta_c$ (see Fig. 2). According to Sec. II B, in the dimensionless system a pulse evolves due to the effective dissipation ($\epsilon_0>0$) and the perturbation ϵ_1 that affects the phase. The dependence of the peak intensity and FWHM of the transmitted pulse on the detuning is shown in Fig. 3. Dots correspond to numerical calculations of NLCMEs (2), while lines are found using Eqs. (25), (26),

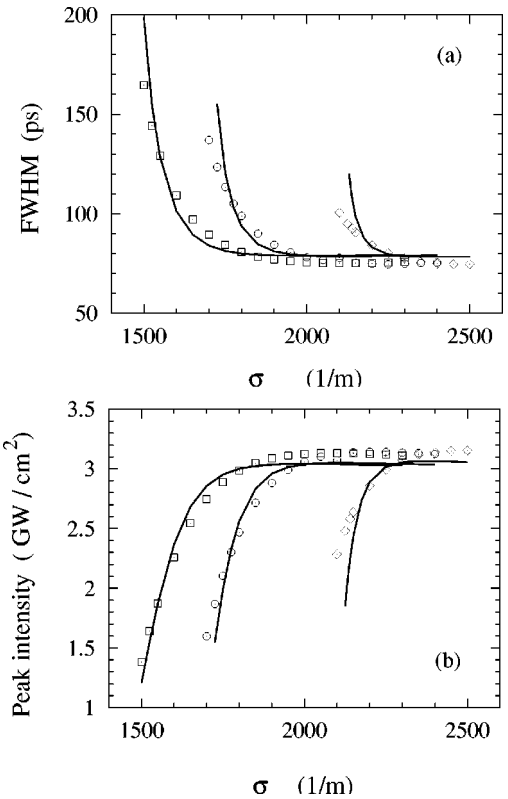

FIG. 3. Dependences of transmitted pulse parameters on the detuning. Dots show the results of numerical calculations of NLCMEs (2), lines correspond to the theory, Eqs. (25), (26), and (23). (a) FWHM, (b) peak intensity. Squares correspond to $\Delta\lambda_c = 0.02$ nm, circles to $\Delta\lambda_c = 0.05$ nm, and diamonds to $\Delta\lambda_c = 0.1$ nm.

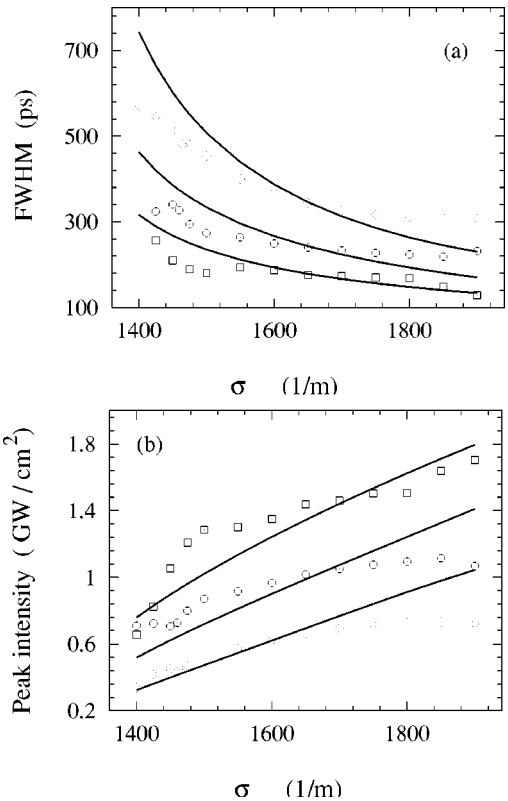

FIG. 4. Dependences of reflected pulse parameters on the detuning. Dots show the results of numerical calculations of NLCMEs (2), lines correspond to the approximate treatment. (a) FWHM, (b) peak intensity. For all plots $\Delta\lambda_c = 0.1$ nm. Squares correspond to $L = 0.06$ cm, circles to $L = 0.12$ cm, and diamonds to $L = 0.30$ cm.

and (23). The peak intensity of the incident pulse is taken $I_{inc} = 3$ GW/cm^2, corresponding to the weakly nonlinear regime, and below the threshold for the two-soliton creation for all detunings considered. For $\Delta\lambda_c = 0.02$ nm and, for example, the detuning $\sigma = 1600$ m^{-1}, the dimensionless lengths are $Z_p(0) = 23.1$, $Z_L = 1.99$, $Z_c(0) = 2.67$, and the coefficients of the perturbations are $\epsilon_0 = 0.187$ and $\epsilon_1 = -0.031$. The condition of the short length is satisfied $Z_L \ll 1/\epsilon_1$, so that the analysis based on Eq. (25) is valid. For large values of the chirp slope, there is appreciable deviation from the theory in the region $\sigma \approx \kappa + \delta_c$, where v is small and the perturbations in Eq. (15) are large. However, in all cases there is good qualitative agreement between the analysis and numerical data.

Though the theory in Sec. II B is developed for pulses in transmission, it can also be used for an estimation of parameters of the reflected pulse at $z = 0$. The dynamics of the pulse can be divided into three stages: (i) the forward propagation in the grating with $\alpha < 0$, (ii) the reflection, and (iii) the backward propagation in the grating with $\alpha > 0$. By using the theory, one can find the pulse parameters for forward propagation up to some point $z_i < z_t$, where z_t is the turning point. The analysis is not valid for the second reflection stage because both the local detuning is close to the edge of the gap and the penetration of the pulse into the gap. However, if one knows the relation between pulse parameters at z_i just before and after the reflection, then one can apply the theory for the final stage of the dynamics as well. We assume that close to the turning point, $z_i \approx 0.9 z_t$, the pulse parameters before and after the reflection are the same.

The result for parameters of the reflected pulses at $z = 0$ for $I_{inc} = 3$ GW/cm^2 is presented in Fig. 4. In order to vary the chirp slope, we keep the total chirp the same for all cases ($\Delta\lambda_c = 0.1$ nm) and change the length of the system L (see also Fig. 2). Using the values $L = 30$ cm and $\sigma = 1700$ m^{-1}, we find $Z_p(0) = 11.6$, $Z_c(0) = 2.01$, $\epsilon_0 = 0.249$, and $\epsilon_1 = -0.028$. The estimate of the turning point position in dimensionless units, which plays the role of Z_L, gives an infinity because the theory does not work for v close to zero. However, the dimensionless length corresponding to z_i is ~ 10. Therefore, we use the Kepler equation (25) for both directions of the pulse propagation in order to compare with numerical results. We choose different values z_i / z_t for different lengths; however, in all cases $z_i / z_t \approx 0.9$ and this ratio is the only fitting parameter in the analysis. We consider the intermediate detunings in the region $[\kappa, \kappa + \delta_c]$ for the following reasons. For detunings $\sigma \approx \kappa$ it is possible to see two-peaked reflected pulses, even for very small initial intensities, i.e., in the linear regime. For detunings $\sigma \approx \kappa + \delta_c$ there is a splitting of the incident pulse into reflected and transmitted pulses near the turning point. Therefore only for the intermediate region of detunings the forward and backward propagating pulses can be considered as a single soliton. The deviation of theoretical lines from results of the numerical calculation in Fig. 4 implies that the change of pulse parameters near the turning point cannot be completely neglected. However, our

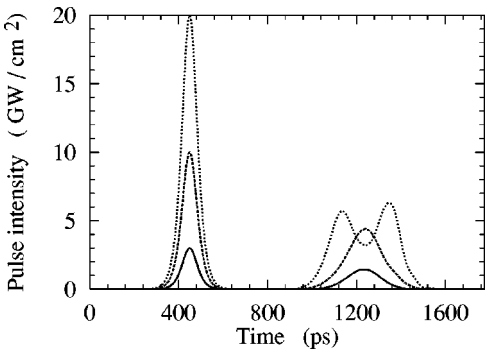

FIG. 5. Time dependences of incident and reflected pulses, the detuning $\sigma = 1700\ \mathrm{m}^{-1}$, and the chirp $\Delta\lambda = 0.1$ nm. The straight line corresponds to $I_{inc} = 3\ \mathrm{GW/cm}^2$, the dashed line to $I_{inc} = 10\ \mathrm{GW/cm}^2$, and the dotted line to $I_{inc} = 20\ \mathrm{GW/cm}^2$.

approach can be used for an approximate evaluation of the reflected pulse parameters.

For large initial peak intensities the reflected pulse splits into two pulses as observed by Slusher *et al.* [9]. Typical profiles of incident and reflected pulses, found from numerical calculations of the NLCMEs, for $\sigma = 1700\ \mathrm{m}^{-1}$ and different intensities are presented in Fig. 5. For such a detuning the transmitted pulses are very weak and they are not shown in the figure. The evolution of the field ($I_{inc} = 20\ \mathrm{GW/cm}^2$) inside the chirped grating during the reflection is shown in Fig. 1. In this case the pulse splitting occurs well before the turning point. Note also that the field intensity near the turning point is large, so that a correct description would probably require additional effects such as higher-order nonlinearities, dispersion, and dissipation.

It follows from Figs. 1 and 5 that the reflected pulse splits when $I_{inc} = 20\ \mathrm{GW/cm}^2$. We found from numerical simulations that the splitting threshold is roughly $16.5\ \mathrm{GW/cm}^2$ for the detuning $\sigma = 1700\ \mathrm{m}^{-1}$. We have found numerically the threshold for the appearance of two pulses in the reflection. As the threshold we used the minimum value of the initial peak intensity, when the peak intensity of the smaller reflected pulse is at least 0.2 of that of the larger one, and the smallest value between the two pulses is less than 0.8 of the peak intensity of the smaller pulse. This choice is not crucial, and thresholds for other definitions are close to the data presented here.

The dependence of the splitting threshold on the detuning, obtained from simulations of the NLCMEs, is shown in Fig. 6.

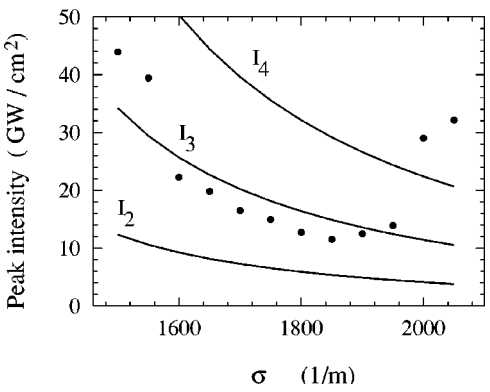

FIG. 6. The splitting threshold versus the detuning. Lines, denoted as I_N, correspond to thresholds of N-soliton creation.

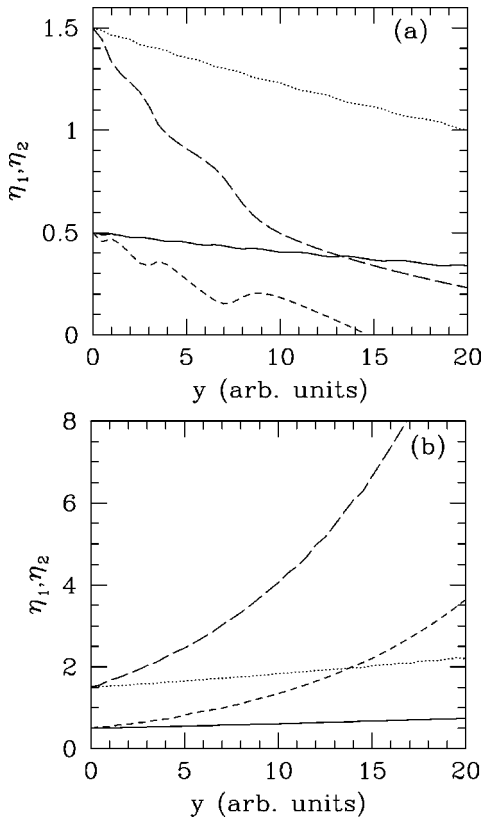

FIG. 7. The variation of imaginary parts η_1 and η_2 for $\epsilon_1 = 0$. (a) $\epsilon_0 = 0.01$, η_1 (dotted line) and η_2 (solid line), $\epsilon_0 = 0.05$, η_1 (long-dashed line) and η_2 (short-dashed line); (b) $\epsilon_0 = -0.01$ and $\epsilon_0 = -0.05$.

6. We also plot the thresholds for two-, three-, and four-soliton creations, calculated from Eq. (12) and initial parameters $v(0)$ and $w(0)$. One can see that the splitting of the reflected pulse is observed if the incident pulse is a multisoliton bound state. Moreover, splitting is observed when the initial peak intensity is close to the threshold for the three-soliton creation, which agrees with the discussion in Sec. II C. The splitting threshold for larger detunings increases because only a fraction of the incident pulse is reflected near the turning point, while the remainder is transmitted. Therefore one needs higher initial intensities to see the splitting for larger detunings. The peak intensity for the three-soliton creation $I_3 = 9I_f/4$ can be used as an estimation for the threshold of the reflected pulse splitting.

IV. CONCLUSION

We have studied the dynamics of nonlinear pulses in the chirped fiber grating. The analysis is based on the NLS limit for the propagation of coupled grating modes. By using soliton perturbation theory, we found the evolution of the parameters of single soliton pulses. The inhomogeneity-induced perturbations lead to changes of the amplitude and width, as well as the phase of the soliton. Namely, a chirped grating with $v_z < 0$ ($v_z > 0$) or in the linearly chirped case with $\alpha < 0$ ($\alpha > 0$) corresponds to the normalized NLS system with a dissipation (an amplification). The variation of the soliton phase results in changes of the soliton velocity. The influence of the perturbations on multisoliton bound

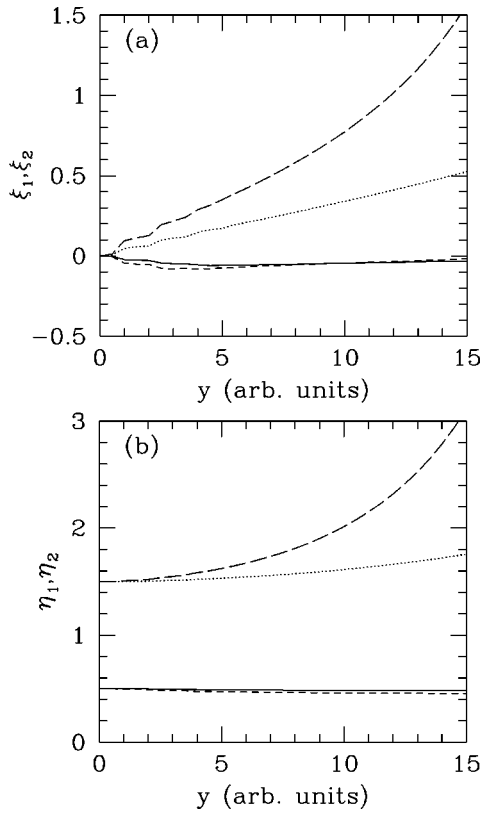

FIG. 8. The variation of eigenvalues λ_1 and λ_2 for $\epsilon_0=0$. (a) Real parts, $\epsilon_1=0.01$, ξ_1 (dotted line), and ξ_2 (solid line); $\epsilon_1=0.02$, ξ_1 (long-dashed line), and ξ_2 (short-dashed line). (b) Imaginary parts η_1, η_2.

states or breathers is also studied. On the basis of this analysis we show that the splitting of the reflected pulse is due to the breaking of the bound multisoliton state. For a better understanding of the reflection process it is necessary to study both the dynamics of pulses for small local detunings and the penetration of pulses into the band gap. Though we consider mainly chirped gratings, the theory can be used for the analysis of the pulse dynamics in any nonuniform gratings with slowly varying parameters.

ACKNOWLEDGMENTS

We are grateful to R. E. Slusher and B. J. Eggleton for discussions. This work is supported by the Australian Research Council.

APPENDIX: DYNAMICS OF A BREATHER. INVERSE SCATTERING APPROACH

Here we study numerically the parameter variation of individual solitons initially bound in a breather using the inverse scattering transform (IST) method. It is known that the initial value problem for the unperturbed NLS equation [Eq. (15) with $\epsilon_0=\epsilon_1=0$] can be solved by this method [19]. This means that the asymptotic behavior of the initial pulse is found from the solution of the associated linear scattering problem. The number N of discrete eigenvalues $\zeta_j=\xi_j+i\eta_j$, where $j=1,\ldots,N$, situated in upper half of the complex plane ($\eta_j>0$), corresponds to the number of emerging solitons. If the solitons are well separated, each of them has the form close to the one-soliton solution

$$\psi(y,\tau)=2\eta\,\mathrm{sech}[2\eta(\tau+2\xi y-\tau_{in})]\times\exp[-2i(\xi\tau-(\xi^2-\eta^2)y+\phi_{in})], \quad \text{(A1)}$$

where τ_{in} and ϕ_{in} are constants. Therefore, $2\eta_j$ and $2\xi_j$ characterize the amplitude (or the width) and the velocity (or the frequency) of the soliton, respectively. However, if the real parts of all ζ_j have the same value, then the solitons form a multi-soliton bound state or a breather. Since individual solitons cannot be distinguished in such a state, the real and imaginary parts of ζ_j lose their simple meaning, so that the breather is described by the whole set of parameters ζ_j. Note that the binding energy is zero [19] and even small perturbations can thus break the state.

We solved Eq. (15) numerically for *constant* ϵ_0 and ϵ_1. At each position y with step $\Delta y=0.5$ we find the discrete spectrum of the associated linear scattering problem. We also check the total number of eigenvalues (solitons). The result for the initial condition (17) with $A=2$ and $\varphi=0$, which corresponds to the discrete spectrum ($N=2$) $\zeta_1=3i/2$ and $\zeta_2=i/2$, is presented in Figs. 7 and 8.

The evolution of η_j, $j=1,2$, under the action of the ϵ_0 term only in Eq. (15) is shown in Fig. 7. The real parts ξ_j remain zero, therefore ϵ_0 does not break the bound state. Note that $\epsilon_0>0$ corresponds to dissipation, while $\epsilon_0<0$ corresponds to gain. The influence of the ϵ_1 term only is presented in Fig. 8. The transformation $\epsilon_1\to-\epsilon_1$ results in exchanging $(\xi_j,\eta_j)\to(-\xi_j,\eta_j)$. As seen from Fig. 8(a) the perturbation ϵ_1 affects the real part ξ_j, breaking the bound state. However, no new solitons are created by the perturbations. The dynamics of individual solitons agrees qualitatively with the dynamics of a single soliton.

[1] C. M. de Sterke and J. E. Sipe, in *Gap Solitons*, edited by E. Wolf, Progress in Optics XXXIII (Elsevier, Amsterdam, 1994), Chap. III, p. 203.
[2] F. Ouellette, Opt. Lett. **12**, 847 (1987).
[3] G. Lenz, B. J. Eggleton, and N. M. Litchinister, J. Opt. Soc. Am. B **14**, 2980 (1997).
[4] A. D. Kersey *et al.*, J. Lightwave Technol. **15**, 1442 (1997).
[5] B. J. Eggleton, C. M. de Sterke, and R. E. Slusher, J. Opt. Soc. Am. B **16**, 587 (1999).
[6] B. J. Eggleton, R. E. Slusher, C. M. de Sterke, P. A. Krug, and J. E. Sipe, Phys. Rev. Lett. **76**, 1627 (1996).
[7] D. Taverner, N. G. R. Broderick, D. J. Richardson, R. I. Laming, and M. Ibsen, Opt. Lett. **23**, 328 (1998).
[8] P. Millar, R. M. De La Rue, T. F. Krauss, J. S. Aitchison, N G. R. Broderick, and D. J. Richardson, Opt. Lett. **24**, 685 (1999).
[9] R. E. Slusher, B. J. Eggleton, T. A. Strasser, and C. M. de Sterke, Opt. Express **3**, 465 (1998).
[10] C. M. de Sterke, J. Lightwave Technol. **17**, 2405 (1999).
[11] C. M. de Sterke, Opt. Express **3**, 405 (1998).
[12] J. Satsuma and N. Yajima, Suppl. Prog. Theor. Phys. **55**,

284 (1974).
[13] G. P. Agrawal, *Nonlinear Fiber Optics* (Academic, San Diego, 1995).
[14] A. I. Maimistov, Zh. Éksp. Teor. Fiz. **104**, 3620 (1993) [JETP **77**, 727 (1993)].
[15] D. Anderson, Opt. Commun. **48**, 107 (1983).
[16] L. D. Landau and E. M. Lifshits, *Mechanics* (Pergamon, Oxford, 1969).
[17] F. Kh. Abdullaev, A. A. Abdumalikov, and B. Baizakov, Kvant. Elektron. (Moscow) **24**, 176 (1997) [Quantum Electron. **27**, 171 (1997)].
[18] C. Desem and P. L. Chu, Opt. Lett. **11**, 248 (1986); K. J. Blow and D. Wood, Opt. Commun. **58**, 349 (1986).
[19] See, e.g., S. Novikov, S. V. Manakov, L. P. Pitaevskii, and V. E. Zakharov, *Theory of Solitons* (Consultants Bureau, New York, 1984).